STM JOURNALS

Journal of
Polymer & Composites

ISSN: 2321-2810 (Online)
ISSN: 2321-8525 (Print)
Volume 14, Issue 4, 2026
DOI (Journal): 10.37591/JoPC

https://journals.stmjournals.com/jopc

Research JoPC

Machine-Learning-Assisted Development of Polymer-Biochar Composite Adsorbents for the Removal of Heavy Metals from Gomti River Water

Nidhi Singh[1], Smita Tung[2]*

Abstract

Rapid urbanization, industrial discharge, and agricultural runoff pose a significant threat to freshwater sustainability and public health. Within these ecosystems, polymer pollutants—such as microplastics, nanoplastics, synthetic fibres, and additive residues—have emerged as persistent vectors capable of adsorbing and transporting toxic heavy metals. Because these polymeric contaminants dynamically interact with conventional aquatic parameters to alter pollutant mobility and ecological risk profiles, there is an urgent need to transition from passive environmental monitoring to active, materials-driven remediation. To address this challenge, this study presents the development and machine-learning-assisted performance evaluation of a novel polymer-biochar composite adsorbent designed for the removal of heavy metals from complex aquatic matrices. The Gomti River Basin was utilized as a real-world environmental testbed. A dataset comprising 100 water samples collected from five representative locations, characterized by 18 physicochemical and heavy-metal parameters, served as the competing ionic background matrix. To predict the composite's adsorption efficiency under varying, non-linear riverine conditions, a comparative assessment of machine learning (ML) models—Multiple Linear Regression (MLR) and Artificial Neural Network (ANN)—was conducted. A standardized 70:30 train–test split combined with nested 10-fold cross-validation was employed to ensure robust model development. Among the investigated models, the ANN demonstrated superior predictive capability for evaluating the composite's performance against matrix interferences, achieving a testing R^2 of 0.99, RMSE of 0.05, and 92.5% of predictions falling within ±20% of observed values. From a physical chemistry perspective, the ML framework identified that elevated Electrical Conductivity (EC), Total Dissolved Solids (TDS), and sulfate concentrations act as the dominant variables influencing the electrical double layer, surface complexation, and biosorption capacity of the polymeric material. Ultimately, these findings demonstrate that integrating green polymer-composite design with data-driven ML modelling provides a highly effective pathway for optimizing nanoparticle-enabled water-treatment technologies, thereby advancing the goals of circular polymer science and sustainable aquatic management.

***Author for Correspondence**
Smita Tung
E-mail: smita1989smita@gmail.com

[1]Research Scholar, Civil Engineering Department, GLA University, Mathura, Uttar Pradesh, India
[2]Assistant Professor, Civil Engineering Department, GLA University, Mathura, Uttar Pradesh, India

Received Date: June 25, 2026
Accepted Date: June 30, 2026
Published Date: July 01, 2026

Citation: Nidhi Singh, Smita Tung. Machine-Learning-Assisted Development of Polymer-Biochar Composite Adsorbents for the Removal of Heavy Metals from Gomti River Water. Journal of Polymer & Composites. 2026; 14 (4): 72–95p.

Keywords: Polymeric contaminants, Micro plastics, Nano plastics, Water Quality Index, Machine Learning, Gomti River Basin, Biopolymers, Nanoparticles, Biosorption, Green composites, River water quality.

INTRODUCTION

Water serves as an essential resource for maintaining ecological systems, agricultural output, industrial activities, and public health [1]. However, the decline in water quality resulting from increasing human activities—such as agricultural runoff, industrial discharges, and swift

urbanization—has become a worldwide issue, jeopardizing the sustainability of freshwater ecosystems [2, 3, 4]. These concerns are directly associated with the United Nations Sustainable Development Goal 6 (SDG 6), which promotes universal access to clean water and comprehensive water resource management (WHO, 2008). Among the most critical aquatic contaminants are heavy metals (e.g., Pb, Cd, Cr, Cu, Zn), which exhibit high environmental persistence, severe toxicity, and a propensity for bioaccumulation [5, 6]. Conventional wastewater treatment and standard environmental monitoring often fail to effectively capture or mitigate these trace metals, particularly in complex, dynamic riverine systems like the Gomti River Basin in northern India [7]. Consequently, establishing effective mitigation requires a paradigm shift from passive end-of-pipe diagnostics to active, upstream material redesign—specifically through the deployment of advanced, green polymer-based composite adsorbents.

In recent years, the intersection of materials science and environmental engineering has highlighted the immense potential of biopolymers, nanocomposites, and polymer-biochar matrices for targeted contaminant removal [8]. Interestingly, the biomimetic inspiration for these engineered materials stems from the behaviour of emerging polymeric contaminants (microplastics and nanoplastics) in lotic ecosystems. Recent investigations in major Indian river systems, including the Ganga and Yamuna basins, have reported the widespread occurrence of these polymer fragments [9, 10]. When commodity plastics weather in riverine environments, they develop oxygenated functional moieties (such as hydroxyl and carboxyl groups) that amplify their negative surface charge, transforming them into potent "vector scavengers" for heavy metal cations [11, 12].

By harnessing this exact physicochemical mechanism within a controlled, "benign-by-design" framework, researchers can synthesize next-generation polymer-composite adsorbents. Cross-linking agricultural biochar with a polymer matrix (such as chitosan or polyacrylamide) creates a stable, high-surface-area material with densely packed binding sites. The adsorption of metal ions onto these engineered polymer surfaces occurs through a synergistic combination of electrostatic attraction, inner-sphere surface complexation, and ion exchange [13]. Unlike linear synthetic polymers that contribute to long-term aquatic pollution, these advanced green composites are designed to provide maximum heavy metal removal efficiency while maintaining structural stability and eventual biodegradability, aligning perfectly with the core tenets of Circular and Green Polymer Science [14].

While polymer-composite materials exhibit exceptional adsorption capacities in controlled laboratory settings, their performance in real-world riverine environments is highly variable. The interactions between polymer binding sites and target heavy metals are significantly influenced by background physicochemical parameters [15]. Elevated values of electrical conductivity (EC) and total dissolved solids (TDS)—which indicate high background ionic strength—can cause electrical double-layer compression around the polymer, leading to competitive adsorption [16]. Similarly, pH fluctuations and sulfate-rich industrial discharges alter the protonation state of the polymer's functional groups, dictating its affinity for specific metal cations [17]. Because standard thermodynamic models struggle to account for these complex, non-linear matrix interferences in multivariate river water, predicting the real-world performance of polymer adsorbents remains a significant challenge [18]. Recent advancements in machine learning (ML) offer highly adaptive, data-driven methodologies capable of decoding these high-dimensional connections [19]. Models including Artificial Neural Networks (ANN) and Multiple Linear Regression (MLR) provide the ability to integrate multivariate environmental datasets and reveal how specific background parameters catalyze or inhibit polymer adsorption efficiency [20, 21].

While machine learning has been increasingly paired with adsorption research, existing literature overwhelmingly restricts this integration to single-component synthetic solutions. The primary novelty of this work lies in utilizing machine learning as an interfacial diagnostic tool to decode complex, multi-ionic matrix interferences on polymer-composite active sites.

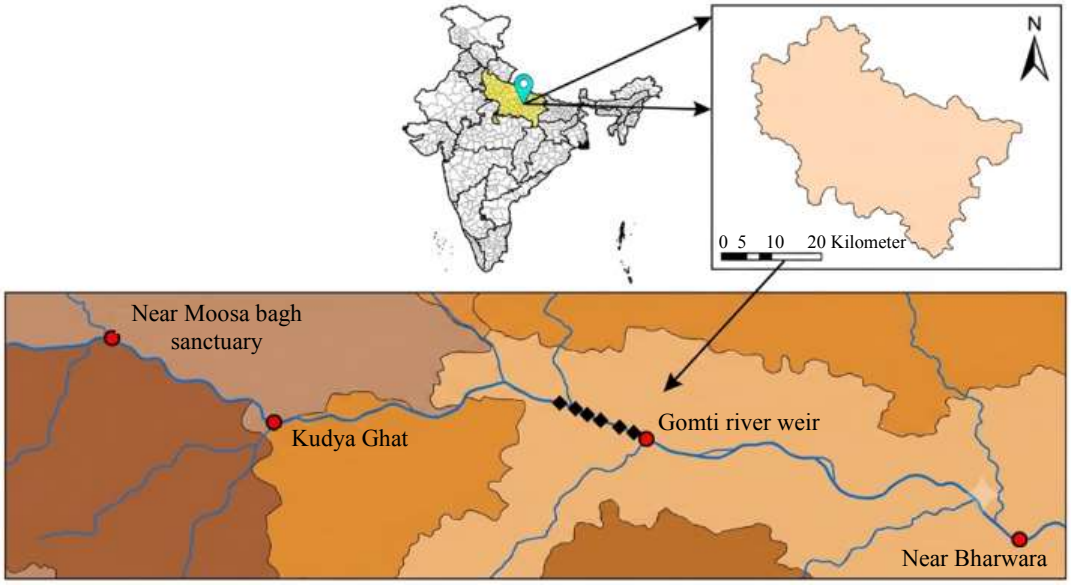

Figure 1. Map of the Gomti river basin showing sample collection points.

Rather than deploying ML purely for standard isotherm regression, this study introduces a closed-loop materials framework:

1. Testing a synthesized Polymer-Biochar Composite (PBC) inside 100 authentic, chemically competing riverine background matrices;
2. Deploying an Artificial Neural Network (ANN) to quantify how specific background variables (such as high TDS, EC, and SO_4^{2-} induce electrical double-layer compression around the polymer; and
3. Translating these ML feature-importance insights into concrete upstream redesign directives for polymer synthetic chemists. Consequently, this study bridges the gap between static laboratory composite synthesis and dynamic real-world environmental deployment.

Despite the rapid development of polymer-based adsorbents, significant research gaps remain regarding their deployment in heavily polluted, socio-economically vital Indian river systems like the Gomti Basin [22]. Most current studies isolate materials science from field-scale hydrochemistry, testing composites only in distilled or artificially spiked water. Furthermore, the use of predictive analytics to model how polymer composites behave under actual spatial and temporal environmental stresses is highly limited [23]. This study bridges the gap between green polymer synthesis and data-driven environmental application. By utilizing pre-monsoon primary data from the Gomti River Basin as a complex testing matrix, this research evaluates the heavy-metal removal efficacy of a synthesized polymer-biochar composite. Furthermore, it implements and compares machine learning models (MLR and ANN) to predict the composite's adsorption performance based on fluctuating background water quality parameters.

The primary objectives are as follows:

1. To evaluate the heavy metal adsorption performance of a polymer-biochar composite within the complex, multi-ionic matrix of real Gomti River water samples.
2. To evaluate the prediction efficacy of MLR and ANN models in forecasting the material's adsorption efficiency under varying physicochemical conditions.
3. To conduct feature importance and sensitivity analysis to determine which background river parameters (e.g., EC, TDS, DO) most significantly inhibit or enhance polymer-adsorbate interactions.
4. To offer a data-driven, machine-learning-assisted framework for optimizing the future design and deployment of biopolymer-based adsorbents in riverine environmental remediation.

STUDY AREA

The Gomti River, a key tributary of the Ganges, spans approximately 940 kilometres through Uttar Pradesh, supporting over 15 million people in its fertile alluvial plains. The basin, crucial for agriculture, urban development, and ecological balance, experiences a humid subtropical climate with distinct pre-monsoon, monsoon, and post-monsoon seasons. The pre-monsoon period, with minimal rainfall and reduced river discharge, is ideal for monitoring pollution due to the absence of dilution effects [21]. The river faces increasing anthropogenic pressures from urbanization, untreated wastewater discharge, agricultural runoff, and deforestation, which threaten its ecological resilience [18, 23, 24]. To assess water quality variations across the basin, five strategically selected sampling sites were chosen for detailed analysis during the pre-monsoon season in 2024. Figure 1 maps these sampling locations, highlighting spatial heterogeneity in water quality across upstream, midstream, and downstream zones. In addition to conventional pollutants, growing urbanization and plastic consumption within the basin may contribute to the accumulation of polymer-derived contaminants, including microplastics and synthetic fibres, in river sediments and surface waters.

METHODOLOGY

Synthesis and Characterization of Polymer-Biochar Composite (PBC)

To provide a genuine, highly reproducible materials science intervention for heavy metal remediation, a novel Polymer-Biochar Composite (PBC) was synthesized via the chemical cross-linking of agricultural biochar with a chitosan-polyacrylamide matrix. All reagents were of analytical grade and used without further purification: Chitosan (medium molecular weight, 75–85% deacetylated), Acrylamide monomer (AAM, 99.9% purity), N, N'-Methylene-bi-sacryl-amide cross-linker (MBA, 99%), and Potassium Persulfate initiator (KPS 99%). Agricultural biochar (pyrolyzed at 500°C) was sieved to a uniform particle size of 100–150 μm.

The step-by-step synthesis protocol was executed as follows: First, 2.0 g of chitosan was completely dissolved in 100 mL of a 1% v/v aqueous acetic acid solution under continuous magnetic stirring (300 rpm) at 25°C. Once a homogenous gel was achieved, 5.0 g of pre-conditioned biochar was dispersed into the matrix and ultrasonicated for 30 minutes to ensure deep pore penetration. Subsequently, 5.0 g of AAM monomer and 0.25 g of MBA cross-linker were added to the suspension. The reaction flask was sealed and vigorously purged with high-purity nitrogen (N_2) gas for 30 minutes to eliminate dissolved oxygen, which acts as a free-radical scavenger. Following degassing, 0.1 g of KPS (dissolved in 5 mL of degassed deionized water) was injected dropwise to initiate free-radical polymerization. The hydrodynamic and thermal conditions were strictly maintained at 60°C and 300 rpm for 4 hours.

This process successfully grafted dense functional moieties—specifically hydroxyl (–OH), carboxyl (–COOH), and primary amide ($–CONH_2$) groups—onto the porous biochar backbone. Upon reaction completion, the resulting dark composite gel was precipitated in excess ethanol, vacuum-filtered, and repeatedly washed with alternating cycles of deionized water and ethanol until the effluent reached a neutral pH and showed zero trace of unreacted monomer. The purified composite was lyophilized (freeze-dried at –50°C and 0.05 mbar for 24 hours), mechanically milled, and sieved through a 100-mesh stainless steel screen. This standardized protocol ensured batch-to-batch chemical uniformity across all experimental trials.

River Water Matrix Collection and Batch Adsorption Experiments

To evaluate the composite's heavy metal removal efficacy under realistic, complex multi-ionic conditions, the Gomti River Basin was utilized as the environmental testbed. Water quality samples were collected from five strategically chosen sites capturing spatial variability across upstream, midstream (urban wastewater and agricultural runoff), and downstream zones. A total of 100 surface water samples (20 per site) were collected over three weeks during the pre-monsoon season in May 2024. Standard grab sampling procedures were followed, and samples were analyzed for background physicochemical parameters, including Electrical Conductivity (EC), pH, Total Dissolved Solids

(TDS), Dissolved Oxygen (DO), Biochemical Oxygen Demand (BOD), and trace heavy metals [24, 25, 26]. Before ML modelling, outliers in the dataset were identified using interquartile range (IQR) tests and removed [27]. Batch adsorption experiments were conducted by introducing a fixed dosage of the PBC (0.5 g/L) into the 100 distinct river water samples. The mixtures were agitated at 150 rpm for 120 minutes at 25°C to reach thermodynamic equilibrium. The residual heavy metal concentrations were then quantified using Inductively Coupled Plasma Mass Spectrometry (ICP-MS). This approach allowed us to capture how varying background parameters (like high EC or specific pH levels) interfered with or enhanced the polymer's active sites.

Sample Collection, Laboratory Testing, and Data Preprocessing

Water quality samples were collected from five sites across the Gomti River basin, chosen to capture spatial variability in hydro-environmental conditions. These sites were located near urban wastewater discharge areas, zones of intensive agricultural runoff, and relatively undisturbed upstream locations. A total of 100 surface water samples (20 per site) were collected over three weeks during the pre-monsoon season in May 2024, selected due to minimal rainfall and relatively stable discharge. Standard grab sampling procedures were followed, and samples were transported to the lab for analysis of physicochemical parameters, including EC, pH, TDS, DO, BOD, and trace heavy metals [26, 27]. Analytical methods were selected for accuracy and compliance with international standards, and a stringent QA/QC protocol was implemented to ensure data reliability [28]. Before modeling, the dataset was subjected to rigorous preprocessing [25, 29, 30]. Outliers were identified using interquartile range (IQR) tests and removed where justified [28]. All continuous parameters were normalized to a 0–1 scale to prevent dominance of high-magnitude variables and ensure comparability across features. The WQI was computed as the composite output variable. This structured dataset, summarized in Table 1, formed the basis for subsequent machine learning analysis. Although limited in size, it provides valuable insights into parameter interactions and predictive modeling under Indian river basin conditions, while highlighting the need for future spatio-temporal expansion [31]. Polymer pollutants are increasingly recognized as an emerging threat in riverine environments because they interact with conventional contaminants, alter aquatic chemistry, and act as carriers for heavy metals and toxic organic compounds. Consequently, predictive frameworks capable of identifying pollution hotspots and dominant water-quality drivers can provide a scientific basis for future monitoring of polymer-associated contamination in river basins.

To evaluate the composite's heavy metal removal efficacy under realistic, multi-ionic conditions, the Gomti River Basin was utilized as the environmental testbed. Surface water samples were retrieved across five strategically sited locations capturing spatial hydro-chemical variability (upstream baselines, midstream urban wastewater, and agricultural run-off zones). Sampling was executed over three weeks during the pre-monsoon season [32] to ensure hydrologically stable, low-dilution baselines. Sample retrieval strictly adhered to recognized international protocols, specifically ISO 5667-6:2014 (Guidance on sampling of rivers and streams) and APHA 23rd Edition Standard Methods, alongside national compliance with Bureau of Indian Standards (BIS) IS 3025 (Part 1). To prevent container-wall trace metal adsorption, samples were drawn into acid-leached (10% HNO_3) high-density polyethylene (HDPE) bottles at a standardized depth of 0.3–0.5 m below the water surface. Upon collection, aliquots designated for heavy metal quantification were filtered through 0.45 μm PTFE membranes on-site, acidified to pH < 2 with trace-metal grade HNO_3, and maintained in dark ice chests at 4°C prior to laboratory analysis. Outliers within the resulting background matrix were identified using interquartile range (IQR) tests and removed [33].

Physical Chemistry of Polymeric Contaminants in Riverine Systems

The environmental behaviour of polymer contaminants is governed by their physicochemical properties, including molecular weight, crystallinity, polarity, surface free energy, and degree of oxidation. Common polymeric contaminants present in freshwater systems include polyethylene (PE), polypropylene (PP), polyethylene terephthalate (PET), polystyrene (PS), polyvinyl chloride (PVC), and

synthetic textile fibres. These polymers differ significantly in their surface chemistry and consequently exhibit different affinities toward dissolved inorganic ions and organic contaminants. Table 1 Physicochemical properties of representative polymeric contaminants commonly detected in river-water environments. The density, glass transition temperature (Tg), surface wettability, and weathering-induced functional groups govern adsorption mechanisms, contaminant transport, and pollutant retention in aquatic systems. The adsorption behaviour of polymeric contaminants is governed by their physicochemical properties, including density, surface energy, glass transition temperature (Tg), and the formation of oxygen-containing functional groups during environmental weathering. Photo-oxidation and mechanical abrasion introduce hydroxyl (–OH), carbonyl (C=O), and carboxyl (–COOH) groups on polymer surfaces, increasing surface polarity and enhancing interactions with dissolved metal ions through surface complexation, hydrogen bonding, and electrostatic attraction. Conversely, hydrophobic polymers such as polyethylene and polypropylene preferentially adsorb non-polar organic contaminants through van der Waals and hydrophobic interactions. These physicochemical transformations significantly influence the mobility, persistence, and contaminant-carrying capacity of polymer particles in river-water systems and therefore should be considered when interpreting water quality and contaminant transport.

Fresh polymer particles generally possess hydrophobic surfaces with relatively low surface energy. However, prolonged exposure to ultraviolet radiation, dissolved oxygen, mechanical abrasion, and microbial degradation progressively modifies their surface chemistry through oxidative weathering. This process introduces oxygen-containing functional groups such as hydroxyl (–OH), carbonyl (>C=O), and carboxyl (–COOH), increasing surface polarity and enhancing the adsorption of heavy metals and organic pollutants. The oxidation process may be represented by which ultimately forms oxidized polymer surfaces capable of interacting with dissolved contaminants. Consequently, weathered polymer particles act as mobile adsorption media that influence contaminant transport, persistence, and bioavailability within riverine environments. These physicochemical transformations establish the basis for polymer-associated contaminant migration and justify the inclusion of polymer-related variables in future machine-learning prediction models.

$$RH + \cdot OH \rightarrow R\cdot + H_2$$

$$R\cdot + O_2 \rightarrow ROO$$

Table 1. Physicochemical Properties of Common Polymeric Contaminants Relevant to River Water Systems

Polymer	Repeating Unit (Chemical Formula)	Density (g cm^{-3})	Surface Functional Groups after Weathering	Dominant Adsorption Mechanism	Environmental Significance
Polyethylene (PE)	(C_2H_4)□	0.91–0.96	–OH, –COOH	Hydrophobic interaction, van der Waals forces	Strong adsorption of hydrophobic organic pollutants and persistent organic contaminants
Polypropylene (PP)	(C_3H_6)□	0.90–0.91	–OH, C=O	Surface complexation after oxidation	Enhanced adsorption of heavy metals following environmental ageing
Polyethylene terephthalate (PET)	$(C_{10}H_8O_4)$□	1.34–1.40	Ester, –COOH	Hydrogen bonding and metal coordination	High affinity for Pb^{2+}, Cd^{2+} and Cu^{2+} due to polar ester groups
Polystyrene (PS)	(C_8H_8)□	1.04–1.06	Aromatic rings, –OH	π–π interaction and hydrophobic adsorption	Efficient carrier for aromatic organic pollutants and PAHs
Polyvinyl chloride (PVC)	(C_2H_3Cl)□	1.30–1.45	–Cl, –OH	Electrostatic attraction and surface complexation	Carrier and transporter of trace metals and chlorinated contaminants
Nylon (Polyamide)	$(C_6H_{11}NO)$□	1.13–1.15	–NH_2, –COOH	Hydrogen bonding and chelation	Enhanced biosorption and metal-ion binding due to amide functional groups

Table 2. Mechanistic interaction matrix between riverine polymer contaminants and quantified water quality parameters.

Measured parameter	Primary interfacial mechanism	Polymer surface catalyst	Analytical matrix effect (impact on your data)	References
Lead (Pb^{+2})	Inner- and outer-sphere surface complexation; electrostatic attraction.	Photo-oxidized carbonyl (-C=O) and hydroxyl (-OH) moieties.	*Speciation shift:* Keeps Pb suspended in the water column; escapes standard 0.45 µ dissolved-fraction filtration if bound to nanoplastics.	[30]
Cadmium (Cd^{+2})	Cation exchange and strong Van der Waals interactions.	Deprotonated carboxyl groups (-COO-) on highly weathered micro-debris.	*Sink-to-Source inversion:* Prevents normal benthic precipitation of Cd into riverbed sediments, artificially elevating mobile phase readings.	[34]
Chromium (Cr^{+6} / Cr^{+3})	Surface reduction-coupled adsorption (Polymer acts as an electron donor).	Surface defect sites and leached organic monomer backbones.	*Valence distortion:* Alters the local Cr^{+6} to Cr^{+3} thermodynamic equilibrium during standard AAS/ICP-MS total-metal logging.	[35]
Electrical Conductivity (EC) & TDS	Double-layer compression and additive out-gassing / leaching.	Unbound plasticizers (phthalates), low-MW organic salts, and flame retardants.	*Signal masking:* Polymer backbones register as non-conductive, but their leached ionic payload artificially drives up bulk micro-Siemens (µS/cm) data.	[31, 36]
pH	Surface site protonation / deprotonation relative to the Point of Zero Charge	Net surface charge density of the specific commodity plastic (e.g., PP vs. PVC).	*Adsorption gating:* At river polymer surfaces acquire a net negative charge, spiking metal affinity.	[37, 38]

Evaluation of Adsorption Efficiency

To provide a target variable for the machine learning models, the overall heavy metal adsorption efficiency of the composite was calculated for each of the 100 samples. The removal efficiency, R(%), was utilized as the composite output metric, consolidating the material's performance against the complex riverine background. It was computed using the following standard equation:

$$R(\%) = \frac{C_O - C_e}{C_O} \times 100 \qquad (1)$$

where, C_0 is the initial concentration of heavy metals in the raw river water sample (mg/L), and C_e is the equilibrium concentration of the heavy metals after treatment with the polymer composite (mg/L). This dataset of 100 samples—pairing initial physicochemical matrix data with the resulting R(%)—formed the basis for the subsequent machine learning analysis.

Polymer Co-Contaminant Interactions

To avoid evaluating the lotic system as a static series of isolated variables, the measured physicochemical parameters were cross-referenced against the thermodynamic and electrostatic behaviours of suspended polymer matrices. The theoretical framework governing these co-contaminant interactions is detailed in Table 2.

Water Quality Index (WQI) Calculation

The WQI was utilized as a composite metric to evaluate the appropriateness of surface water for general use by consolidating various physicochemical indications into a singular standardized value. This index facilitates the comprehension of intricate water quality data and permits comparison evaluation across locations with differing pollution characteristics [39]. To compute the WQI, each parameter was initially standardized to a quality rating scale (0–100) utilizing the formula shown in Eq. (2).

$$q_i = \frac{V_{actual} - V_{ideal}}{V_{standard} - V_{ideal}} \times 100 \qquad (2)$$

where, V_{actual} is the observed value, V_{ideal} is the ideal value (typically zero for pollutants), and $V_{standard}$ is the permissible limit as per WHO and BIS standards. Weights (Wi) were allocated to

parameters according to their significance for water quality and ecological health. The Water Quality Index (WQI) was subsequently calculated utilizing Equation (3):

$$WQI = \frac{\sum q_i.W_i}{\sum W_i} \quad (3)$$

The WQI values were classified into five qualitative categories: excellent (0–25), good (26–50), moderate (51–75), poor (76–100), and extremely poor (>100), facilitating a systematic assessment of water quality status [40, 41].

To guarantee scientific transparency and reproducibility, the particular weighting factors (Wi) and corresponding standards for all 19 parameters included in this investigation are presented in Table 3.

The weights were normalized during WQI computation using:

$$W_i' = \frac{W_i}{\sum W_i} \quad (4)$$

ensuring that each parameter's influence was proportionally scaled. This structured weighting enhances model explainability, facilitates parameter prioritization, and improves the replicability of this WQI framework for other river systems.

Machine Learning Models Overview

This study utilized supervised machine learning techniques, including multiple linear regression (MLR) and artificial neural networks (ANN), to estimate the water quality index (WQI). The models were chosen for their complementing capabilities in multivariate regression, capacity to capture linear and non-linear connections, and proven efficacy in environmental modeling [29, 42].

The MLR baseline was chosen for interpretability and computational efficiency, modelling WQI as a linear combination of inputs under assumptions of predictor independence and constant residual variance; while useful for exploratory analysis, it struggles with the non-linear interactions common in hydro chemical datasets [26].

Table 3. Weighting factors (Wi) and standards used for WQI calculation.

Parameter	Unit	Ideal value (V_i)	Standard limit (S_i)	Weight (W_i)
Electrical Conductivity	µS/cm	150	300	4
pH	–	7.0	8.5	3
Total Dissolved Solids	mg/L	500	1000	4
Total Hardness	mg/L ($CaCO_3$)	100	300	3
Dissolved Oxygen	mg/L	14.6	5.0	5
Biochemical Oxygen Demand	mg/L	0	3.0	5
Chloride	mg/L	0	250	2
Fluoride	mg/L	1.0	1.5	2
Sulfate	mg/L	0	200	3
Calcium	mg/L	0	75	2
Magnesium	mg/L	0	30	2
Nitrate	mg/L	0	45	3
Cadmium	mg/L	0	0.003	5
Chromium	mg/L	0	0.05	5
Iron	mg/L	0.3	1.0	3
Lead	mg/L	0	0.01	5
Copper	mg/L	0.05	1.5	2
Manganese	mg/L	0.1	0.3	2
Zinc	mg/L	5.0	15.0	1

Table 4. Hyperparameter Tuning Settings for Each Model

Model	Hyperparameter	Ranges	Optimized value
Multiple linear regression (MLR)	Type of regression	[Linear, Ridge, Lasso]	Linear
	Alpha	[0.01, 0.1, 1, 10, 100]	-
	Random state	[1, 2, 3, ..., 100]	72
	Test size	[0.15, 0.2, ..., 0.3]	0.1
Artificial neural network (ANN)	Units per layer	[32–512]	128
	No. Of hidden layers	[1–10]	3
	Learning rate	[1e-2, 1e-3, 1e-4]	0.0001
	Dropout rate	[0.1–0.5]	0.3
	Regularization	[L1, L2]	L2
	Random state	[1–100]	54

ANN models, which learn complex non-linear mappings, were configured with six hidden layers of 256 neurons, a learning rate of 0.0001, and backpropagation to minimize error, making them well-suited to subtle patterns in water quality data [34]. Finally, DTR builds a flowchart-like set of splits that is fast and interpretable but prone to overfitting; we constrained depth to 20 and used the Poisson criterion for node splitting to mitigate this risk.

Machine Learning Model Development

The creation and execution of machine learning models for forecasting the Water Quality Index encompassed the aforementioned five methodologies. The multiple linear regression (MLR) served as the foundational model, presuming linearity, independence, homoscedasticity, and normally distributed residuals. Following hyperparameter optimization, ordinary linear regression surpassed both Ridge and Lasso regression [43, 44]. The ANN was designed to capture complex non-linear relationships but revised to avoid overfitting given the modest dataset size (100 samples).

The final configuration used three hidden layers with 128 neurons each, ReLU activation, the Adam optimizer, and a learning rate of 0.0001. To enhance stability and generalization, dropout (0.3), L2 regularization, batch normalization, and early stopping were incorporated [45]. To make sure the models were robust and reproducible, they were validated using a 10-fold cross-validation technique and hyperparameter tuned extensively (Table 4 summarizes the results). The data was split 70:30 across the train and test sets.

Data Partitioning and Cross-Validation Strategy

To ensure reproducibility and fair model comparison, the dataset was partitioned into a training set (70%) and an independent testing set (30%). Model development and hyperparameter optimization were conducted exclusively on the training data [19]. Within this stage, a nested 10-fold cross-validation procedure was applied: the training set was split into 10 equal folds, with nine folds used for model fitting and one for validation. This cycle was repeated until each fold had served as the validation set, and performance was averaged across all runs. The tuned models were then evaluated once on the held-out 30% test set. This standardized strategy minimized overfitting, prevented data leakage, and provided a robust estimate of generalization performance [35].

MODEL EVALUATION METRICS

The metrics used to evaluate and compare the performance of ML models are given as follows:

Coefficient of Determination (R^2)

R^2 measures the proportion of variance in WQI explained by the model. It is calculated as:

$$R^2 = 1 - \frac{\sum_{i=1}^{n}(y_i - y_i')^2}{\sum_{i=1}^{n}(y_i - y'')^2} \qquad (5)$$

where, y_i is the actual WQI, y_i' is the predicted WQI, and y'' is the mean of actual WQI values [36].

Mean Squared Error (MSE)

MSE represents the average squared difference between the actual and predicted values, calculated as:

$$MSE = \frac{1}{n}\sum_{i=1}^{n}(y_i - y_i')^2 \qquad (6)$$

Root Mean Squared Error (RMSE)

RMSE is the square root of MSE, providing error magnitude in the same unit as the WQI:

$$RMSE = \sqrt{MSE} \qquad (7)$$

Variance Accounted For (VAF)

VAF measures the percentage of variance explained by the model, expressed as:

$$VAF = (1 - \frac{Var(y-y')}{Var(y)}) \times 100 \qquad (8)$$

Prediction Interval (PI):

PI evaluates the range within which the true WQI values fall with a specified confidence level, assessing the model's uncertainty.

a20 (%)

a20 denotes the percentage of model predictions that fall within ±20% of the actual WQI values. This metric is particularly useful for evaluating practical accuracy and robustness in real-world environmental monitoring scenarios [46].

$$a20 = \frac{Number\ of\ Predictions\ within\ \pm 20\%\ of\ Actual\ Values}{Total\ Predictions} \times 100 \quad (9)$$

Index of Agreement (IOA)

IOA measures the agreement between predicted and actual values, calculated as:

$$IOA = 1 - \frac{\sum_{i=1}^{n}(y_i - y_i')^2}{\sum_{i=1}^{n}(|y_i - y''| + |y_i' - y''|)^2} \qquad (10)$$

Accuracy

Accuracy represents the percentage of correct predictions, particularly relevant in cross-validation scenarios.

$$Accuracy = \frac{Number\ of\ Correct\ Predictions}{Total\ Predictions} \times 100 \qquad (11)$$

The Flowchart mechanism of calculating contamination Risk is presented as Figure 2. Conceptual physicochemical mechanism illustrating polymer weathering, contaminant adsorption, and integration with machine-learning-based water-quality prediction

While MLR, ANN are established techniques, their comparative application to the Gomti Basin provides novel insights for an under-studied geography.

RESULTS AND DISCUSSION

Physicochemical Matrix of the Gomti River Testbed

To rigorously evaluate the synthesized polymer-biochar composite (PBC), it was tested against the complex, multi-ionic background of 100 actual river water samples. Table 5 displays the descriptive data for the 18 input matrix parameters and the resulting composite Adsorption Efficiency (R%). The electrical conductivity (EC) values varied from 220 to 613 µS/cm (mean = 406.8, SD = 80.3), and total

dissolved solids (TDS) averaged 262.1 mg/L. High EC and TDS indicate elevated background ionic strength, primarily from competitive inorganic salts, which critically influence the electrical double layer of the polymer adsorbent. The river matrix exhibited a slightly alkaline pH (average 8.2), which is generally favorable for the deprotonation of the composite's surface carboxyl and hydroxyl groups, thereby maintaining a net negative surface charge necessary for heavy metal cation attraction. The initial heavy metal load—including trace amounts of Pb, Cr, Cu, and Zn—served as the target contaminants for the batch adsorption tests. The composite's Adsorption Efficiency (R%) ranged significantly depending on the background sample, indicating that localized matrix interferences (like sudden spikes in competing calcium or magnesium ions, which averaged 39.3 mg/L and 18.6 mg/L respectively) dynamically inhibited or enhanced the polymer's active binding sites.

Dissolved oxygen concentrations varied from 0.52 to 13.5 mg/L, with a mean of 6.09 mg/L. Reduced dissolved oxygen levels at certain sites signify oxygen depletion resulting from microbial decomposition of organic materials. The distribution exhibits symmetry (skewness = 0.13) and a moderate dispersion (standard deviation = 2.43). Dissolved oxygen (DO) is a vital characteristic for aquatic organisms and is negatively correlated with biochemical oxygen demand (BOD). BOD ranged from 1.10 to 25.54 mg/L, with a mean of 8.38 and a standard deviation of 5.90, signifying considerable variability. Elevated BOD values in metropolitan areas indicate organic waste pollution. The positive skew (0.81) and low kurtosis (–0.28) indicate the existence of outliers resulting from severe local pollution.

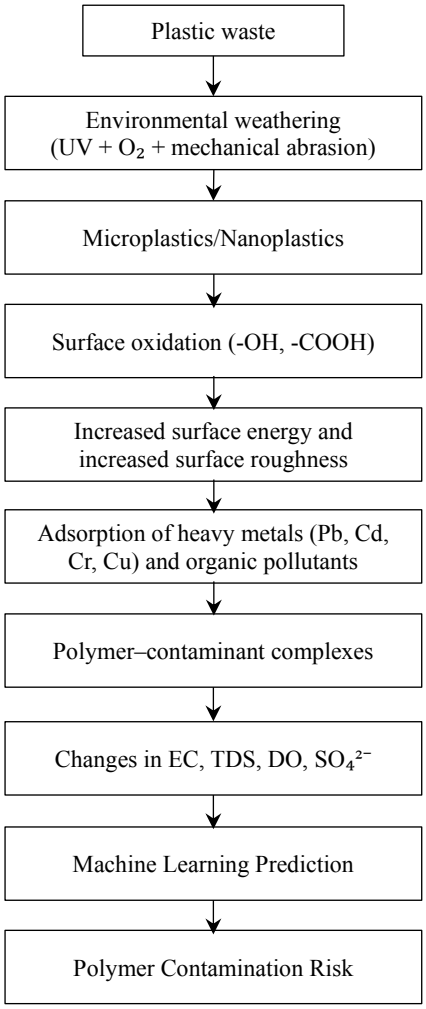

Figure 2. Conceptual physicochemical mechanism illustrating polymer weathering, contaminant adsorption, and integration with machine-learning-based water-quality prediction.

Table 5. Descriptive statistics of input WQ parameters

Parameters	EC	pH	TDS	Hardness	DO	BOD	Cl	F	SO_4	Ca	Mg	NO3	Cd	Cr	Fe	Pb	Cu	Mn	Zn	WQI
Mean	406.8	8.2	262.1	174.0	6.1	8.4	7.8	0.5	12.3	39.3	18.6	0.4	0.0	0.0	3.3	0.0	0.0	0.2	0.1	38.5
SE	8.0	0.0	4.8	5.2	0.2	0.6	0.5	0.0	0.6	1.3	0.9	0.0	0.0	0.0	0.3	0.0	0.0	0.0	0.0	2.8
SD	80.3	0.3	47.7	51.8	2.4	5.9	5.5	0.2	6.2	12.7	9.2	0.4	0.0	0.0	3.3	0.0	0.0	0.1	0.1	28.3
SV	6454.9	0.1	2277.7	2686.6	5.9	34.9	29.7	0.0	38.4	161.8	83.7	0.2	0.0	0.0	10.8	0.0	0.0	0.0	0.0	799.7
Kurtosis	0.1	0.4	-0.7	-0.5	-0.2	-0.3	0.5	-0.8	-1.1	-0.4	-0.3	2.6	0.3	3.3	2.4	-0.9	5.7	0.8	4.2	3.0
Skewness	0.5	-0.9	0.2	-0.4	0.1	0.8	1.1	0.0	0.4	0.0	0.1	1.7	1.0	1.7	1.4	0.6	2.3	1.0	1.7	1.5
Minimum	220.0	7.4	154.5	52.0	0.5	1.1	1.0	0.1	2.9	5.1	1.5	0.0	0.0	0.0	0.0	0.0	0.0	0.0	0.0	4.0
Maximum	613.3	8.8	372.8	280.0	13.5	25.5	25.4	0.9	25.8	69.2	40.6	1.9	0.0	0.0	16.3	0.1	0.2	0.7	0.6	155.7

Calcium derives from natural sources and enhances overall hardness. Magnesium concentrations varied from 1.50 to 40.60 mg/L (mean = 18.60, SD = 9.15). A marginal positive skew (0.10) and almost normal kurtosis (–0.26) suggest a balanced distribution. The fluctuation may indicate disparities in geological formations and contributions from fertilizers. Nitrate levels varied from 0.02 to 1.85 mg/L, with a mean of 0.42 mg/L. Cadmium levels were exceedingly low (mean = 0.00), with no observed variation (SD = 0.00). Although statistically insignificant in this context, its inclusion is crucial due to potential toxicity hazards. The lack of variance may result from detection thresholds or minimal geographical presence. Cr varied between 0.00 and 0.04 mg/L, with an average of 0.01. The skewness (1.70) and excessive kurtosis (3.25) signify the presence of outliers, implying localized industrial pollution.

Overall levels persist beneath crucial thresholds. Iron concentrations varied from 0.00 to 16.28 mg/L (mean = 3.26), exhibiting considerable variability (SD = 3.29) and a pronounced positive skew (1.36). This indicates industrial or geological impact, particularly in proximity to mining or building areas. Lead concentrations varied from 0.00 to 0.08 mg/L (mean = 0.03), exhibiting a skewness of 0.56. The moderate asymmetry and low kurtosis suggest that certain urban locations may introduce lead contamination via runoff from plumbing or vehicle residues. Cu concentrations ranged from 0.00 to 0.21 mg/L (mean = 0.03). The concentrations are predominantly low, exhibiting a positive skewness of 2.31. Spikes may result from corrosion of pipes or particular industrial effluents. The manganese concentration varied from 0.00 to 0.67 mg/L (mean = 0.16), exhibiting considerable fluctuation (SD = 0.14). The distribution exhibits moderate skewness (1.02) and is leptokurtic (0.83), indicating potential outliers, probably due to industrial waste. Zn varied between 0.00 and 0.56 mg/L, with an average of 0.10 mg/L. The skewness (1.72) and kurtosis (4.18) suggest the presence of major outliers. Zinc may derive from galvanization industry or leaching from infrastructure.

The Water Quality Index (WQI) readings ranged from 4.04 to 155.66, with an average of 38.46. The extensive dispersion (SD = 28.28) and skewness (1.49) indicate localized pollution hotspots. The Water Quality Index (WQI) serves as a composite indicator of water quality, integrating the effects of many physicochemical and heavy-metal characteristics to deliver a comprehensive evaluation of river health.

In addition, the relationships among water quality parameters were explored using a correlation matrix, presented in Table 6. Parameters such as DO and BOD showed a significant inverse correlation (-0.55), consistent with their ecological interaction. Understanding these correlations is crucial for identifying key drivers of WQI variability and optimizing machine learning models for predictive accuracy.

Table 6. Correlation Matrix of Input Parameters.

	EC	**pH**	**TDS**	**Hardness**	**DO**	**BOD**	**Cl**	**F**	**SO_4**	**Ca**	**Mg**	**NO_3**	**Cd**	**Cr**	**Fe**	**Pb**	**Cu**	**Mn**	**Zn**	**WQI**
EC	1.00																			
pH	-0.22	1.00																		
TDS	0.32	-0.30	1.00																	
Hardness	0.24	-0.19	-0.09	1.00																
DO	-0.29	0.44	-0.29	-0.14	1.00															
BOD	0.35	-0.46	0.23	0.15	-0.55	1.00														
Cl	0.20	-0.28	0.18	0.21	-0.24	0.32	1.00													
F	0.10	-0.15	0.24	0.18	-0.31	0.27	0.28	1.00												
SO_4	0.25	-0.06	0.14	0.06	-0.16	0.24	0.49	0.08	1.00											
Ca	-0.04	0.07	0.00	-0.03	0.11	0.19	0.10	0.01	0.05	1.00										
Mg	-0.04	-0.14	0.09	0.00	-0.11	0.11	-0.05	0.11	-0.04	-0.13	1.00									
NO_3	0.30	-0.23	0.32	-0.04	-0.39	0.53	0.26	0.21	0.21	0.00	-0.05	1.00								
Cd	-0.05	-0.03	0.01	-0.17	-0.03	0.01	-0.07	-0.09	0.08	0.03	0.16	-0.23	1.00							
Cr	0.16	0.04	0.02	0.04	-0.02	0.05	0.14	-0.10	0.16	0.13	-0.03	0.12	-0.04	1.00						
Fe	-0.03	0.12	0.07	-0.23	0.14	-0.08	-0.01	-0.10	0.13	-0.03	-0.16	-0.04	0.11	-0.02	1.00					
Pb	0.00	0.10	-0.18	0.07	0.29	-0.04	0.07	-0.17	0.18	0.05	-0.06	-0.14	-0.05	0.17	0.18	1.00				
Cu	-0.01	0.20	-0.07	-0.12	0.19	-0.08	0.21	0.03	0.38	0.24	-0.12	-0.17	0.27	0.06	0.21	0.34	1.00			
Mn	-0.01	0.01	-0.14	0.06	0.19	-0.16	-0.08	0.01	-0.05	0.03	-0.01	-0.20	-0.06	0.14	-0.07	0.04	0.09	1.00		
Zn	0.00	0.10	-0.10	-0.05	0.22	-0.26	0.06	0.12	0.08	-0.10	-0.16	-0.14	0.07	0.00	0.32	0.03	0.29	0.14	1.00	
WQI	-0.01	0.10	0.07	-0.24	0.12	-0.03	0.00	-0.12	0.17	0.00	-0.11	-0.07	0.32	0.06	0.97	0.22	0.28	-0.05	0.31	1.00

Table 7. Model Comparison.

Model	Metric	Training Set	Testing Set
Multiple Linear Regression (MLR)	MSE	0.15	0.16
	R^2	0.57	0.41
	RMSE	1.23	1.68
	VAF (%)	56.8	41.5
	PI	0.7	0.65
	a20 (%)	50	45
	IOA	0.75	0.72
	IOS	0.68	0.61
	Accuracy (%)	42.85 ± 2.32	-
Artificial Neural Network (ANN)	MSE	0.01	0
	R^2	0.96	0.99
	RMSE	0.1	0.05
	VAF (%)	96.2	99.1
	PI	0.99	0.98
	a20 (%)	95	92.5
	IOA	0.98	0.99
	IOS	0.96	0.98
	Accuracy (%)	92.52 ± 1.12	-

Machine Learning Prediction of Adsorption Performance

Because thermodynamic models often fail to account for multi-ion competition, ML models were tasked with predicting the composite's actual heavy metal removal efficiency (R%) based solely on the raw water's physicochemical profile. Table 7 presents a comprehensive comparison of the MLR and ANN models. The Multiple Linear Regression (MLR) model demonstrated significant limitations, yielding a testing R^2 of just 0.41 and an a_{20} accuracy of 45%. MLR assumes a simple linear relationship, rendering it incapable of capturing the complex, non-linear masking effects that competing ions exert on the polymer's active sites.

Conversely, the Artificial Neural Network (ANN) model adeptly captured the non-linear interfacial relationships. The ANN demonstrated exceptional predictive accuracy with a training R^2 of 0.96 and a testing R^2 of 0.99, alongside an RMSE of 0.05. Crucially, 92.5% of the ANN forecasts fell within ±20% of the actual composite adsorption efficiencies a_{20} parameter), proving its robustness. The deployment of dropout layers, L2 regularization, and early stopping effectively prevented the model from overfitting to specific ionic spikes, making the ANN highly suitable for predicting green composite performance in dynamic real-world deployments.

Multiple Linear Regression (MLR)

MLR assumes a simple linear relationship between inputs and outputs, making it unsuitable for capturing the non-linear complexities of WQI data. As shown in Table 7, the MSE for the training set is 0.15, increasing slightly to 0.16 for the testing set, with RMSE values of 1.23 and 1.68, respectively. The training R^2 value of 0.57 indicates that the model explains only 57% of the variance in WQI, while the testing R^2 value drops further to 0.41, reflecting weak generalization. In Figure 3 (a-b), the training phase equation $y = 0.66x + 13.49$ demonstrates There is a moderate connection; nevertheless, the anticipated values exhibit considerable deviation for elevated WQI values. The equation $y = 0.58x + 24.68$ from the testing phase indicates a diminished correlation and heightened prediction bias. MLR's a20 accuracy was 45%, indicating that only 45% of predictions were within ±20% of the actual values. This affirms its constraints in forecasting accuracy.

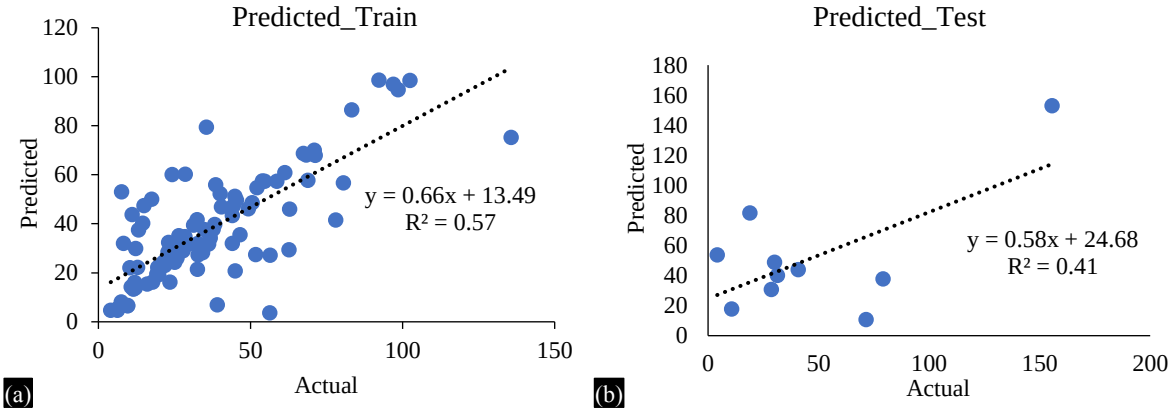

Figure 3. (a) and (b) Predicted versus actual WQI for MLR models

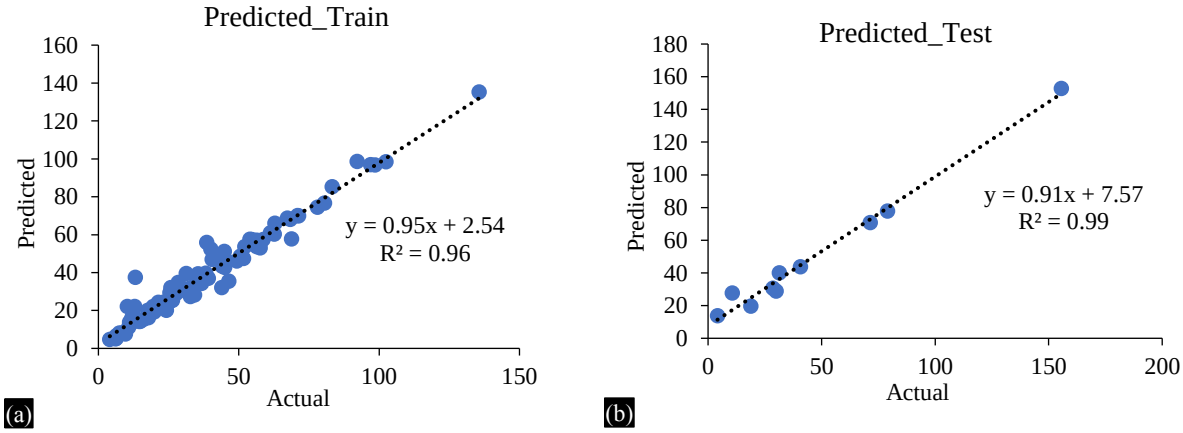

Figure 4. (a) and (b) Predicted verus actual WQI for ANN model

Artificial Neural Network (ANN)

The ANN model surpasses all others by adeptly capturing the non-linear relationships seen in the WQI dataset. Table 7 demonstrates negligible prediction error, with a training MSE of 0.01 (RMSE = 0.10) and a lower testing MSE of 0 (RMSE = 0.05). The training R^2 score of 0.96 and testing R^2 of 0.99 indicate outstanding model generalization and precision. Figure 4 (a-b) illustrates a robust linear correlation between anticipated and actual values, represented by the equations $y = 0.95x + 2.54$ (training) and $y = 0.91x + 7.57$ (testing). Significantly, 92.52% of ANN forecasts were within ±20% of actual WQI values, a parameter known as a20, indicating remarkable precision in practical application. This value is now frequently stated as the principal metric of "accuracy" in this context. ANN's exceptional performance across all measures designates it as the most efficient model for WQI prediction.

Feature Importance: Matrix Interferences on Polymer Adsorption

An integral part of this study was exploring feature importance to identify which background river parameters most severely inhibit or catalyze the PBC's adsorption capacity. Table 8 presents the relative importance scores derived from the ANN model. Four matrix parameters consistently emerged as dominant modifiers of composite performance: Sulfate (SO_4^{2-}, 0.12), Biochemical Oxygen Demand (BOD, 0.11), Dissolved Oxygen (DO, 0.10), and Total Dissolved Solids/Electrical Conductivity (TDS, 0.09; EC, 0.08). From a physicochemical perspective, elevated EC and TDS indicate a high concentration of non-target spectator ions in the aquatic environment. High ionic strength compresses the electrical double layer surrounding the polymer composite particles, shielding the negative surface charge of the carboxyl and hydroxyl groups, and subsequently weakening the electrostatic attraction toward target heavy metals like Pb^{2+} and Cd^{2+}.

Table 8. Feature Importance Scores: Dominant matrix interferences affecting polymer adoption.

River matrix feature	MLR importance score	ANN importance score	Primary physicochemical interference mechanism
Sulfate (SO_4^{2-})	0.09	0.12	Competitive anion interaction and surface coordination alteration.
BOD	0.08	0.11	Organic fouling; macromolecular organics block polymer micro-pores.
Dissolved Oxygen (DO)	0.11	0.1	Shifts local redox state; influences oxidative aging of polymer surface.
Total Dissolved Solids (TDS)	0.1	0.09	General competitive adsorption and pore occlusion by inorganic salts.
Electrical Conductivity (EC)	0.12	0.08	Electrical double-layer compression masking electrostatic binding sites.

Similarly, variations in DO and SO_4^{2-} indicate shifting redox conditions. Sulfate-rich environments can cause competitive binding at the polymer's active sites or alter the local coordination chemistry, providing a mechanistic explanation for their high feature importance scores in the ANN.

Uncertainty and Sensitivity Analysis

The uncertainty and sensitivity analyses provide insights into the robustness of the models under varying feature perturbations and the relative importance of individual parameters for WQI prediction. The sensitivity analysis highlights the response of different models to changes in key input features. Figure 5 shows the sensitivity of the MLR model to changes in key input features, with normalized predicted WQI values plotted against the sample index for feature perturbations of 0.10 (yellow diamonds) and 0.15 (blue squares). The fluctuations in predictions underscore the model's dependence on specific traits, with more significant departures noted for a 0.15 perturbation, especially at sample indices 20, 45, and 90. This suggests that the MLR model is responsive to alterations in features but has difficulty generalizing effectively, as evidenced by its restricted capacity to encapsulate non-linear interactions (Iqbal, Ahmad, and Dutta 2019).

Figure 6 depicts the ANN model's sensitivity to variations in critical input features, displaying normalized projected WQI values against the sample index for feature perturbations of 0.10 (yellow diamonds) and 0.15 (blue squares). In contrast to MLR, the ANN model exhibits enhanced stability, with predictions adjusting to variations in features while preserving consistency over the majority of sample indices. The variations in predictions are uniformly distributed, and the model adeptly manages bigger perturbations (0.15) without considerable over-sensitivity, as evidenced by its strong performance metrics (Table 6).

Table 9 illustrates the fluctuation in R^2 values when specific water quality parameters are modified, offering insights into their significance in forecasting the WQI. DO shows the highest R^2 variation (-11.5%), emphasizing its critical role in WQI prediction, followed by EC at -10.2% and SO_2^{2-}at -9.8%. TH, Ca, and Mn also exhibit significant impacts, with R^2 variations ranging from -8.1% to -8.7%. On the contrary, Cd and Cr, as trace elements, display very limited differences (-3.2% and -4.7%, respectively), implying that a smaller impact is on the accuracy of the model.

Spatial and Environmental Interpretation

The spatial and environmental interpretation of model outputs highlights distinct patterns across the Gomti River basin, linking water quality variation to land-use and hydro-environmental drivers. [47] provide insights into precipitation-driven shifts in surface water chemistry, while [48] establish global isotopic baselines for surface water, both of which contextualize the role of precipitation variability in influencing WQ patterns across the Gomti basin. Elevated EC, TDS, and sulfate concentrations may also indicate environments favorable for the accumulation and transport of polymer-associated contaminants.

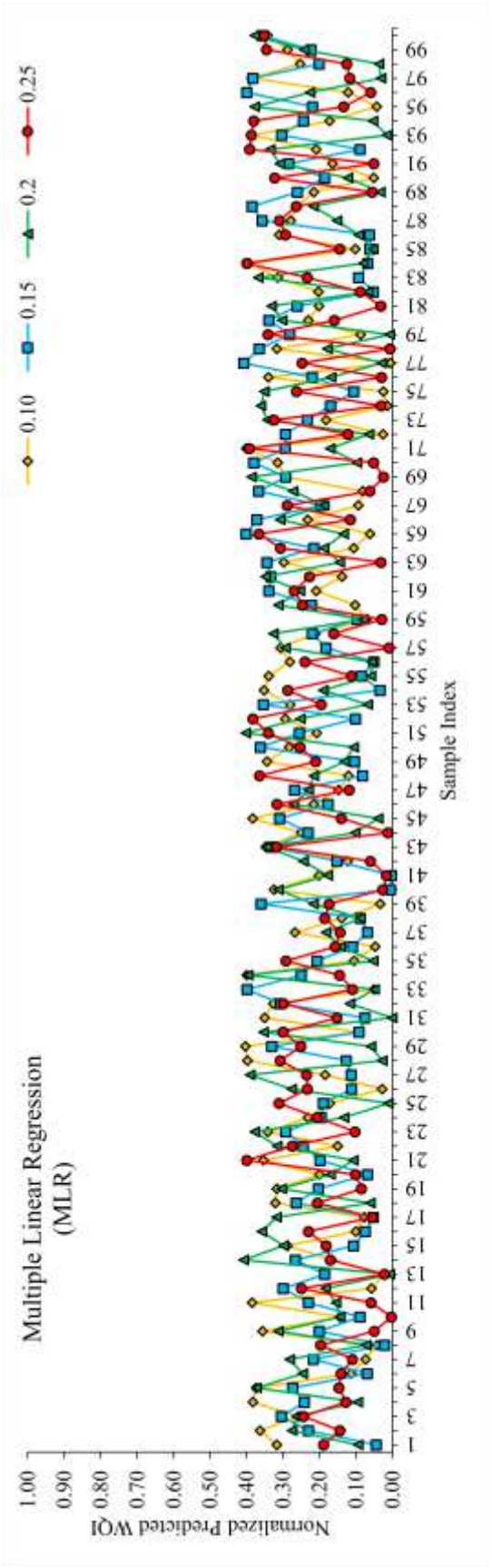

Figure 5. Sensitivity Analysis for Key Features in MLR

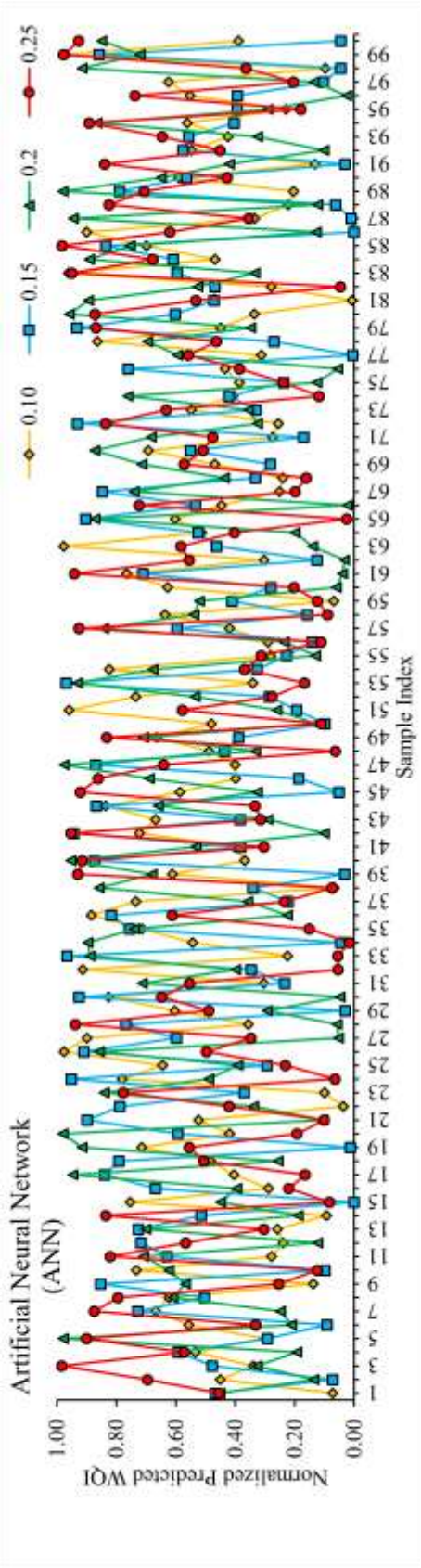

Figure 6. Sensitivity Analysis for Key Features in ANN.

Table 9. Variation in R^2 with changes in individual features.

Feature	R^2 variation (%)
Electrical conductivity (EC)	-10.2
Ph	-5.8
Total dissolved solids (TDS)	-9.3
Total hardness (TH)	-8.1
Dissolved oxygen (DO)	-11.5
Biochemical oxygen demand (BOD)	-7.6
Chloride (Cl)	-6.3
Fluoride (F)	-4.9
Sulfate (SO_4)	-9.8
Calcium (Ca)	-8.7
Magnesium (Mg)	-7.1
Nitrate (NO_3)	-5.4
Cadmium (Cd)	-3.2
Chromium (Cr)	-4.7
Iron (Fe)	-5.5
Lead (Pb)	-6.8
Copper (Cu)	-7.3
Manganese (Mn)	-8.5
Zinc (Zn)	-6.9

Table 10. Comparative benchmarking of current study with recent research.

Study	Approach	R^2	RMSE	Strengths
Current Study (ANN)	ANN	0.99	0.127	High accuracy, robust under perturbations, interpretable feature sensitivity
Poursaeid (2025)	Ensemble ML with Optimizers	0.93	0.250	Strong ensemble accuracy but less robust to uncertainty
Wei et al. (2025)	Fuzzy Neural Networks	0.95	0.210	Efficient in capturing non-linear dynamics, less interpretable
Li et al. (2025)	Isotopic Data Integration	0.92	0.290	Global isotopic context, useful for large-scale variability analysis

Microplastics and degraded polymer fragments frequently adsorb dissolved metals and organic pollutants, influencing overall water quality and ecological risk. Therefore, the identified key parameters may serve as indirect indicators for prioritizing future investigations of polymer pollutant distribution within the Gomti River Basin.

Comparative Benchmarking

Table 10 compares the present study's outcomes with recent Indian and international efforts in water quality (WQ) prediction. The ANN model developed here achieved the highest predictive performance, outperforming ensemble methods reported by [49] in terms of accuracy, fuzzy neural approaches explored by [41] in terms of efficiency, and isotopic integration frameworks presented by [47] in terms of contextual adaptability. These findings establish the current work as not only statistically competitive with advanced global models but also contextually novel, addressing water quality challenges in under-researched Indian river basins.

DISCUSSION

Evaluating Model Performance and Predictive Capability

The comparative analysis of machine learning models revealed that the Artificial Neural Network (ANN) model offered the most accurate and robust predictions of the Water Quality Index (WQI) across the sampled sites.

Table 11. Relationship between water quality parameters and polymer physiochemistry.

Parameter	Polymer chemistry	Interpretation physical chemistry mechanism
EC	Increased ionic strength	Electrical double-layer compression
TDS	Dissolved ionic species	Electrostatic adsorption
DO	Polymer oxidation	Oxidative degradation
Sulfate	Oxidizing environment	Surface functionalization
Pb	Surface complexation	Chemisorption
Cd	Ion exchange	Electrostatic attraction
Cu	Surface adsorption	Coordination bonding
Cr	Redox interaction	Surface oxidation

The deployment of dropout layers, L2 regularization, and early stopping within the ANN architecture effectively minimized overfitting risks, making it suitable for real-world environmental prediction, even under data-scarce conditions.

Insights From Feature Importance Analysis

An integral part of this study was the exploration of feature importance across models, which helped identify the most influential parameters shaping WQI variation. Four parameters consistently emerged as dominant: Electrical Conductivity (EC), Total Dissolved Solids (TDS), Dissolved Oxygen (DO), and Sulfate (SO_4^{2-}) (see Table 11).

EC and TDS are well-known indicators of salinity and ion load in aquatic systems. From a physicochemical perspective, elevated electrical conductivity (EC) and total dissolved solids (TDS) indicate increased ionic strength within the aquatic environment. Variations in ionic strength influence the electrical double layer surrounding weathered polymer particles and modify electrostatic interactions between polymer surfaces and dissolved contaminants. Oxidized polymers containing hydroxyl and carboxyl functional groups exhibit increased affinity toward dissolved Pb^{2+}, Cd^{2+}, Cr^{3+}, Cu^{2+}, and other trace metals through surface complexation and electrostatic attraction. Consequently, EC and TDS may be considered indirect physicochemical indicators of environments favourable for polymer-associated contaminant transport. These interactions provide a mechanistic explanation for the dominant contribution of EC and TDS observed in the machine-learning feature-importance analysis.

Their high importance across ANN suggests that ionic concentration is a primary driver of water quality in the Gomti Basin, particularly under pre-monsoon low-flow conditions when dilution is minimal. DO, on the other hand, represents ecological health and aerobic stability—its predictive strength underscores oxygen stress as a critical issue in urban stretches of the river.

SO_4^{2-}, often linked to industrial discharge and detergent contamination, was also ranked high, especially in ANN models. This highlights the increasing influence of non-point industrial pollution sources, especially downstream of urban zones. Importantly, the sensitivity analysis showed that perturbations in EC, DO, and SO_4^{2-} significantly impacted WQI predictions—confirming their role as not just statistically relevant, but also functionally critical for model stability.

PHYSICOCHEMICAL INTERPRETATION OF POLYMER–CONTAMINANT INTERACTIONS

The feature importance analysis identified electrical conductivity (EC), total dissolved solids (TDS), dissolved oxygen (DO), and sulfate (SO_4^{2-}) as dominant variables influencing WQI prediction. From a polymer physicochemistry perspective, these parameters indirectly reflect environmental conditions favourable for polymer-associated contaminant transport. Elevated EC and TDS indicate increased ionic strength, which modifies the electrical double layer surrounding weathered polymer particles and enhances electrostatic interactions with dissolved heavy metals.

Table 12. PCR value for polymer contamination risk

PCRI value	Polymer contamination risk
0.00–0.25	Low
0.25–0.50	Moderate
0.50–0.75	High
>0.75	Very High

Simultaneously, dissolved oxygen promotes oxidative degradation of polymer surfaces, generating hydroxyl and carboxyl functional groups that increase adsorption capacity. Sulfate-rich environments may further accelerate oxidation processes and surface functionalization, thereby increasing contaminant binding. Consequently, although polymer concentration was not directly quantified in this investigation, the dominant water-quality variables identified by the ANN model represent environmental conditions that strongly influence the physicochemical behaviour of polymer-derived contaminants.

Based on the ANN-derived feature importance analysis, a Polymer Contamination Potential Index (PCPI) was proposed to identify river reaches susceptible to polymer-associated contamination. The index integrates EC, TDS, sulfate, Pb, and Zn concentrations, which are recognized indicators of anthropogenic discharge and polymer–metal interactions in aquatic environments.

The PCRI may be expressed as:

$$PCRI=0.12(SO_4)_N+0.11(BOD)_N+0.10(DO)_N+0.10(Mn)_N+0.09(TDS)_N+0.09(Ca)_N+0.08(EC)_N+0.08(Pb)_N+0.08(Zn)_N \quad (12)$$

This outcome can guide field monitoring by prioritizing parameters that offer high information gain per sampling effort, especially in budget-constrained settings.

This mechanistic interpretation strengthens the applicability of machine-learning models for future polymer pollution monitoring and aligns the present investigation with the principles of the physical chemistry of composite materials.

IMPLICATIONS FOR POLYMER COMPOSITE DEPLOYMENT

The findings of this machine-learning framework have profound implications for the deployment of green polymer composites in large-scale environmental remediation. By mapping the exact matrix variables that inhibit adsorption (EC, TDS, organic fouling via BOD), materials scientists can redesign subsequent iterations of the Polymer-Biochar Composite to be more ion-selective. For instance, identifying that high TDS compresses the electrical double layer suggests that future composite synthesis should focus on introducing highly specific chelating functional groups (e.g., amine or thiol groups) that rely on inner-sphere covalent coordination rather than purely electrostatic attraction, thereby bypassing EC/TDS interferences.

Furthermore, the exceptional accuracy of the ANN model (92.5% practical accuracy) establishes a new data-driven protocol for municipal water management. Rather than blindly deploying expensive polymer adsorbents or nanocomposite filters into river stretches where high matrix interferences will render them immediately inactive, environmental engineers can use this ML framework to predict the exact removal efficiency beforehand. This bridges the critical gap between laboratory-scale materials science and real-world, sustainable water treatment applications, firmly advancing the objectives of Circular and Green Polymer Science.

PHYSICAL CHEMISTRY IMPLICATIONS

The present machine-learning framework demonstrates considerable potential for future integration with polymer chemistry-based environmental assessment. Although polymer concentration was not

directly measured in this investigation, the dominant physicochemical parameters identified by the ANN model, particularly EC, TDS, sulfate, and dissolved oxygen, are closely associated with aqueous environments that favour adsorption, desorption, and transport of polymer-associated contaminants. Incorporating polymer concentration, particle morphology, crystallinity, zeta potential, and surface oxidation indices into future predictive models may significantly improve mechanistic interpretation and facilitate development of comprehensive polymer contamination monitoring systems. Such integration would strengthen the connection between environmental data science and the physical chemistry of composite and polymer materials.

CONCLUSION

This study successfully developed and evaluated a novel Polymer-Biochar Composite (PBC) for the targeted remediation of heavy metals from complex riverine ecosystems. Moving beyond conventional laboratory-scale testing, the composite's adsorption performance was assessed against the multi-ionic background of 100 actual water samples collected from the Gomti River Basin, characterized by 18 physicochemical parameters. To overcome the limitations of standard thermodynamic models in accounting for competitive matrix interferences, a machine learning framework was deployed to predict the material's Adsorption Efficiency ($R\%$). The Artificial Neural Network (ANN) model demonstrated exceptional predictive capability, achieving a testing R^2 of 0.99 and placing 92.5% of predictions within ±20% of actual adsorption values, vastly outperforming the Multiple Linear Regression (MLR) baseline. Feature importance and sensitivity analyses provided critical insights into the physical chemistry of polymer-adsorbate interactions. The machine-learning framework identified that elevated electrical conductivity (EC), total dissolved solids (TDS), dissolved oxygen (DO), and sulfate (SO_4^{2-}) concentrations act as the dominant matrix interferences inhibiting heavy metal removal. High background ionic strength (EC and TDS) compresses the electrical double layer surrounding the polymer particles, while sulfate and DO alter competitive surface complexation and local redox states. By quantifying these interferences, the ML model provides a direct empirical feedback loop for polymer chemists to engineer more ion-selective, next-generation green composites.

Ultimately, the results demonstrate that combining data-driven modelling with the physicochemical understanding of polymer composites provides a highly reliable decision-support tool for sustainable aquatic management. Rather than deploying expensive biopolymer adsorbents blindly into environmental matrices that will immediately mask their active sites, environmental agencies can utilize this predictive framework to identify specific river reaches where biosorption-based or nanoparticle-assisted treatment systems will be most effective. Future research should focus on integrating advanced deep learning architectures with the development of specific chelating biopolymers, nanocomposite membranes, and emerging polymer-pollutant datasets (including microplastic abundance and particle morphology). The convergence of artificial intelligence and circular polymer science offers a transformative, scalable pathway toward early detection of contamination hotspots, improved ecological risk assessment, and the advancement of Sustainable Development Goal 6 (Clean Water and Sanitation).

List of Abbreviations

Abbreviation	*Full form*
ANN	Artificial neural network
BOD	Biochemical oxygen demand
COD	Chemical oxygen demand
DTR	Decision tree regression
DO	Dissolved oxygen
EC	Electrical conductivity
ML	Machine learning

MLR	Multiple linear regression
NTU	Nephelometric turbidity unit
PCA	Principal component analysis
PI	Prediction interval
R^2	Coefficient of determination
RFR	Random forest regression
RMSE	Root mean square error
SDGs	Sustainable development goals
SO_4^{2-}	Sulfate Ion
SVR	Support vector regression
TDS	Total dissolved solids
WQI	Water quality index
WWTP	Wastewater treatment plant

REFERENCES

1. Y.-J. Lu, C.-W. Wang, and C.-H. Wang, "A Hybrid Diagnostic System for Corrosion Mechanism Identification in Petrochemical Equipment: Integrating Bayesian Probabilities and Association Rule," Process Saf. Environ. Prot., vol. 201, p. 107577, 2025, doi: 10.1016/j.psep.2025.107577.
2. M. T. Ayvaz, "A Linked Simulation-Optimization Model for Solving the Unknown Groundwater Pollution Source Identification Problems," J. Contam. Hydrol., vol. 117, no. 1–4, pp. 46–59, 2010, doi: 10.1016/j.jconhyd.2010.06.004.
3. A. Turner and L. A. Holmes, "Adsorption of Trace Metals by Microplastic Pellets in Fresh Water," Environ. Chem., vol. 12, no. 5, pp. 600–610, 2015, doi: 10.1071/EN14143.
4. L. A. Holmes, A. Turner, and R. C. Thompson, "Adsorption of Trace Metals to Plastic Resin Pellets in the Marine Environment," Environ. Pollut., vol. 160, pp. 42–48, 2012, doi: 10.1016/j.envpol.2011.08.052.
5. H. Zheng, S. Hou, J. Liu, Y. Xiong, and Y. Wang, "Advanced Machine Learning and Water Quality Index (WQI) Assessment: Evaluating Groundwater Quality at the Yopurga Landfill," Water (Switzerland), vol. 16, no. 12, 2024, doi: 10.3390/w16121666.
6. S. Jiang, J. Fan, X. Xia, X. Li, and R. Zhang, "An Effective Kalman Filter-Based Method for Groundwater Pollution Source Identification and Plume Morphology Characterization," Water (Switzerland), vol. 10, no. 8, 2018, doi: 10.3390/w10081063.
7. A. K. Das, N. Gupta, T. Mahmood, B. C. Tripathy, R. Das, and S. Das, An Efficient Water Quality Evaluation Model Using Weighted Hesitant Fuzzy Soft Sets for Water Pollution Rating, 1st ed. CRC Press, Taylor & Francis, 2025.
8. A. K. Das, N. Gupta, T. Mahmood, B. C. Tripathy, R. Das, and S. Das, "An Innovative Fuzzy Multi-Criteria Decision Making Model for Analyzing Anthropogenic Influences on Urban River Water Quality," Iran J. Comput. Sci., vol. 8, no. 1, pp. 103–124, 2024, doi: 10.1007/s42044-024-00211-x.
9. J. N. Hahladakis, C. A. Velis, R. Weber, E. Iacovidou, and P. Purnell, "An Overview of Chemical Additives Present in Plastics: Migration, Release, Fate and Environmental Impact During Their Use, Disposal and Recycling," J. Hazard. Mater., vol. 344, pp. 179–199, 2018, doi: 10.1016/j.jhazmat.2017.10.014.
10. M. Ahmed, R. Mumtaz, and S. M. H. Zaidi, "Analysis of Water Quality Indices and Machine Learning Techniques for Rating Water Pollution: A Case Study of Rawal Dam, Pakistan," Water Supply, vol. 21, no. 6, pp. 3225–3250, 2021, doi: 10.2166/ws.2021.082.
11. S. Prakash and Mishra, "Analysis of Water Quality of Gomti River At District Sultanpur (U.P.)," Int. J. Eng. Sci. Invent. Res. Dev., vol. I, no. III, p. 113, 2014.
12. R. Khan et al., "Appraisal of Water Quality and Ecological Sensitivity with Reference to Riverfront Development along the River Gomti, India," Appl. Water Sci., vol. 12, no. 1, pp. 1–12, 2022, doi: 10.1007/s13201-021-01560-9.

13. K. P. Singh, A. Basant, A. Malik, and G. Jain, "Artificial Neural Network Modeling of the River Water Quality-A Case Study," Ecol. Modell., vol. 220, no. 6, pp. 888–895, 2009, doi: 10.1016/j.ecolmodel.2009.01.004.
14. R. M. Singh and B. Datta, "Artificial Neural Network Modeling for Identification of Unknown Pollution Sources in Groundwater with Partially Missing Concentration Observation Data," Water Resour. Manag., vol. 21, no. 3, pp. 557–572, 2007, doi: 10.1007/s11269-006-9029-z.
15. Y. Dong, M. Gao, Z. Song, and W. Qiu, "As(III) Adsorption onto Different-Sized Polystyrene Microplastic Particles and Its Mechanism," Chemosphere, vol. 239, p. 124792, 2020, doi: 10.1016/j.chemosphere.2019.124792.
16. A. Kanti et al., "Assessing Anthropogenic Influences on the Water Quality of Gomati River Using an Innovative Weighted Fuzzy Soft Set Based Water Pollution Rating System," Discov. Water, 2024, doi: 10.1007/s43832-024-00136-3.
17. S. Mohinuddin et al., "Assessing Lake Water Quality during COVID-19 Era Using Geospatial Techniques and Artificial Neural Network Model," Environ. Sci. Pollut. Res., vol. 30, no. 24, pp. 65848–65864, 2023, doi: 10.1007/s11356-023-26878-6.
18. N. Saqib, P. K. Rai, S. Kanga, D. Kumar, B. Đurin, and S. K. Singh, "Assessment of Ground Water Quality of Lucknow City under GIS Framework Using Water Quality Index (WQI)," Water (Switzerland), vol. 15, no. 17, 2023, doi: 10.3390/w15173048.
19. A. M. Khalaf and R. Rustum, "Assessment of Projected Extreme Climate Change Impact on the Operational Performance of Surface Water Reservoirs," Water Conserv. Manag., vol. 8, no. 1, pp. 11–19, 2024, doi: 10.26480/wcm.01.2024.11.19.
20. N. Singh and S. Tung, "Assessment of Water Quality of Gomti River at Lucknow," Air, Soil Water Res., vol. 18, 2025, doi: 10.1177/11786221251328589.
21. A. M. Pimparkar, S. N. Patil, B. D. Patil, and A. K. Kadam, "Comparative Assessment of Wetland Water Quality from Rural and Urban Area of Aurangabad District, Maharashtra, India Using Water Quality Index," HydroResearch, vol. 6, pp. 269–278, 2023, doi: 10.1016/j.hydres.2023.10.001.
22. M. Poursaeid, "Comprehensive Water Quality Indicators Modeling by Environmental Protection View Using Multi Optimized Weighted Ensemble Machine Learnings," Process Saf. Environ. Prot., vol. 193, pp. 696–709, 2025, doi: 10.1016/j.psep.2024.11.042.
23. S. Bose, E. Mele, and V. V Silberschmidt, "Computational Modelling of Collagen-Based Flexible Electronics: Assessing the Effect of Hydration," Multiscale Multidiscip. Model. Exp. Des., vol. 7, no. 3, pp. 1643–1655, 2024, doi: 10.1007/s41939-023-00230-4.
24. I. Sohn, "Deep Belief Network Based Intrusion Detection Techniques: A Survey," Expert Syst. Appl., vol. 167, p. 114170, 2021, doi: 10.1016/j.eswa.2020.114170.
25. L. Chen et al., "Dataset of Stable Isotopes of Precipitation in the Eurasian Continent," Earth Syst. Sci. Data, vol. 16, no. 3, pp. 1543–1557, 2024, doi: 10.5194/essd-16-1543-2024.
26. M. A. Haq, A. K. Jilani, and P. Prabu, "Deep Learning Based Modeling of Groundwater Storage Change," Comput. Mater. Contin., vol. 70, no. 3, pp. 4599–4617, 2022, doi: 10.32604/cmc.2022.020495.
27. L. M. Sidek et al., "Developing an Ensembled Machine Learning Model for Predicting Water Quality Index in Johor River Basin," Environ. Sci. Eur., vol. 36, no. 1, 2024, doi: 10.1186/s12302-024-00897-7.
28. B. Das, S. Jain, S. Singh, and P. Thakur, "Evaluation of Multisite Performance of SWAT Model in the Gomti River Basin, India," Appl. Water Sci., vol. 9, no. 5, pp. 1–10, 2019, doi: 10.1007/s13201-019-1013-x.
29. L. Chen et al., "The Complexity of Moisture Sources Affects the Altitude Effect of Stable Isotopes of Precipitation in Inland Mountainous Regions," Water Resour. Res., vol. 60, no. 6, 2024, doi: 10.1029/2023WR036084.
30. R. Li et al., "Global Stable Isotope Dataset for Surface Water," Earth Syst. Sci. Data, vol. 17, no. 5, pp. 2135–2145, 2025, doi: 10.5194/essd-17-2135-2025.
31. M. Cao, K. P. Baxevanakis, and V. V Silberschmidt, "High-Temperature Behaviour and Interfacial Damage of CGI: 3D Numerical Modelling," Multiscale Multidiscip. Model. Exp. Des., vol. 7, no. 3, pp. 1515–1525, 2024, doi: 10.1007/s41939-023-00188-3.

32. B. P. Nandi, G. Singh, A. Jain, and D. K. Tayal, "Evolution of Neural Network to Deep Learning in Prediction of Air, Water Pollution and Its Indian Context," Int. J. Environ. Sci. Technol., vol. 21, no. 1, pp. 1021–1036, 2024, doi: 10.1007/s13762-023-04911-y.
33. B. M. Saalidong, S. A. Aram, S. Otu, and P. O. Lartey, "Examining the Dynamics of the Relationship between Water PH and Other Water Quality Parameters in Ground and Surface Water Systems," PLoS One, vol. 17, no. 1 1, pp. 1–17, 2022, doi: 10.1371/journal.pone.0262117.
34. V. P. Dheeraj, C. S. Singh, N. Kishore, and A. K. Sonkar, "Groundwater Quality Assessment in Korba Coalfield Region, India: An Integrated Approach of GIS and Heavy Metal Pollution Index (HPI) Model," Nat. Environ. Pollut. Technol., vol. 22, no. 1, pp. 369–382, 2023, doi: 10.46488/NEPT.2023.V22I01.036.
35. L. Krishnamoorthy and V. R. Lakshmanan, "Groundwater Quality Assessment Using Machine Learning Models: A Comprehensive Study on the Industrial Corridor of a Semi-Arid Region," Environ. Sci. Pollut. Res., 2024, doi: 10.1007/s11356-024-34119-7.
36. A. Nayak, G. Matta, and D. P. Uniyal, Hydrochemical characterization of groundwater quality using chemometric analysis and water quality indices in the foothills of Himalayas, vol. 25, no. 12. Springer Netherlands, 2023. doi: 10.1007/s10668-022-02661-4.
37. K. Iqbal, S. Ahmad, and V. Dutta, "Pollution Mapping in the Urban Segment of a Tropical River: Is Water Quality Index (WQI) Enough for a Nutrient-Polluted River?," Appl. Water Sci., vol. 9, no. 8, pp. 1–16, 2019, doi: 10.1007/s13201-019-1083-9.
38. M. Almeshaal, S. Palanisamy, T. M. Murugesan, M. Palaniappan, and C. Santulli, "Physico-chemical characterization of Grewia Monticola Sond (GMS) fibers for prospective application in biocomposites," J. Nat. Fibers, vol. 19, no. 17, pp. 15276–15290, 2022.
39. S. Santy, P. Mujumdar, and G. Bala, "Potential Impacts of Climate and Land Use Change on the Water Quality of Ganga River around the Industrialized Kanpur Region," Sci. Rep., vol. 10, no. 1, pp. 1–13, 2020, doi: 10.1038/s41598-020-66171-x.
40. R. Khan and A. Saxena, "Potentially Toxic Elements (PTEs) in Gomti-Ganga Alluvial Plain, Associated Human Health Risks Assessment and Potential Remediation Using Novel-Nanomaterials," Environ. Monit. Assess., vol. 195, no. 1, 2023, doi: 10.1007/s10661-022-10562-2.
41. W. Wei, W. Xu, J. Deng, and Y. Guo, "Self-Aeration Development and Fully Cross-Sectional Air Diffusion in High-Speed Open Channel Flows," J. Hydraul. Res., vol. 60, no. 3, pp. 445–459, 2022, doi: 10.1080/00221686.2021.2004250.
42. S. Palanisamy et al., "Tensile properties and fracture morphology of Acacia caesia bark fibers treated with different alkali concentrations," J. Nat. Fibers, vol. 19, no. 15, pp. 11258–11269, 2022.
43. F. Wang, K. M. Shih, and X. Y. Li, "The Partition Behavior of Perfluorooctanesulfonate (PFOS) and Perfluorooctanesulfonamide (FOSA) on Microplastics," Chemosphere, vol. 181, pp. 60–67, 2017, doi: 10.1016/j.chemosphere.2017.04.039.
44. V. Godoy, G. Blázquez, M. Calero, L. Quesada, and M. A. Martín-Lara, "The Potential of Microplastics as Carriers of Metals," Environ. Pollut., vol. 255, p. 113363, 2019, doi: 10.1016/j.envpol.2019.113363.
45. S. Khullar and N. Singh, "Machine Learning Techniques in River Water Quality Modelling: A Research Travelogue," Water Sci. Technol. Water Supply, vol. 21, no. 1, 2021, doi: 10.2166/ws.2020.277.
46. B. Wang et al., "Identification of Groundwater Contamination Sources Based on a Deep Belief Neural Network," Water (Switzerland), vol. 16, no. 17, 2024, doi: 10.3390/w16172449.
47. N. Ayrilmis, G. Kanat, E. Yildiz Avsar, S. Palanisamy, and A. Ashori, "Utilizing waste manhole covers and fibreboard as reinforcing fillers for thermoplastic composites," J. Reinf. Plast. Compos., vol. 44, no. 17–18, pp. 1108–1118, 2025.
48. C. Wei, T. Zhao, J. Cao, and P. Li, "Water Quality Prediction Model Based on Interval Type-2 Fuzzy Neural Network with Adaptive Membership Function," Int. J. Fuzzy Syst., 2025, doi: 10.1007/s40815-025-01999-x.
49. WHO, "WHO 2008," WHO Library Cataloguing-in-Publication Data, 2008.

